DNA Sequence Dependent Binding Modes of 4',6-Diamidino-2-phenylindole (DAPI)†

W. David Wilson,*,‡ Farial A. Tanious,‡ Henryk J. Barton,‡ Robert L. Jones,§ Keith Fox,∥ Roman L. Wydra,‡ and Lucjan Strekowski‡

Department of Chemistry and Laboratory for Microbial and Biochemical Sciences, Georgia State University, Atlanta, Georgia 30303, Department of Chemistry, Emory University, Atlanta, Georgia 30322, and Department of Physiology and Pharmacology, School of Biochemical and Physiological Sciences, University of Southampton, Bassett Crescent East, Southampton SO9 3TU, U.K.

Received March 23, 1990; Revised Manuscript Received May 31, 1990

ABSTRACT: The interactions of DAPI with natural DNA and synthetic polymers have been investigated by hydrodynamic, DNase I footprinting, spectroscopic, binding, and kinetic methods. Footprinting results at low ratios (compound to base pair) are similar for DAPI and distamycin. At high ratios, however, GC regions are blocked from enzyme cleavage by DAPI but not by distamycin. Both poly[d(G-C)]$_2$ and poly[d(A-T)]$_2$ induce hypochromism and shifts of the DAPI absorption band to longer wavelengths, but the effects are larger with the GC polymer. NMR shifts of DAPI protons in the presence of excess AT and GC polymers are significantly different, upfield for GC and mixed small shifts for AT. The dissociation rate constants and effects of salt concentration on the rate constants are also quite different for the AT and the GC polymer complexes. The DAPI dissociation rate constant is larger with the GC polymer but is less sensitive to changes in salt concentration than with the AT complex. Binding of DAPI to the GC polymer and to poly[d(A-C)]·poly[d(G-T)] exhibits slight negative cooperativity, characteristic of a neighbor-exclusion binding mode. DAPI binding to the AT polymer is unusually strong and exhibits significant positive cooperativity. DAPI has very different effects on the bleomycin-catalyzed cleavage of the AT and GC polymers, a strong inhibition with the AT polymer but enhanced cleavage with the GC polymer. All of these results are consistent with two totally different DNA binding modes for DAPI in regions containing consecutive AT base pairs versus regions containing GC or mixed GC and AT base pair sequences. The binding mode at AT sites has characteristics which are similar to those of the distamycin–AT complex, and all results are consistent with a cooperative, very strong minor groove binding mode. In GC and mixed-sequence regions the results are very similar to those observed with classical intercalators such as ethidium and indicate that DAPI intercalates in DNA sequences which do not contain at least three consecutive AT base pairs.

Aromatic diamidines, such as 4',6-diamidino-2-phenylindole (DAPI,[1] Figure 1), berenil, and stilbamidine, show a variety of biological effects including antibiotic, antitypanosomal, and antiviral activity, and they are important tools in molecular biology and cytochemistry (Latt, 1979; Gale et al., 1981; Zimmer & Wahnert, 1986). The fluorescence quantum yield of DAPI is very strongly enhanced by AT base pair sequences, and it is widely used as a specific fluorescence marker for chromosomal DNA (Kapuscinski & Szer, 1979; Cavatorta et al., 1985).

Studies with DAPI–DNA complexes have clearly shown that DAPI exhibits an array of interactions of varying strength and specificity with DNA (Zimmer & Wahnert, 1986; Dervan, 1986; Pullman & Pullman, 1981; Kapuscinski & Szer, 1979; Manzini et al., 1983; Kubista et al., 1987; Portugal & Waring, 1988). Complexes with DAPI bound in the minor groove, in the major groove, and by intercalation have been proposed on the basis of a variety of experimental observations with different DNA samples. Footprinting experiments at low ratios indicate a strong protection of AT base pair sequences by DAPI with a binding site size of three to four base pairs (Portugal & Waring, 1988). The protected regions in footprinting experiments are similar to those observed for AT-specific, minor groove binding molecules such as netropsin and Hoechst 33258 (Portugal & Waring, 1988; Jorgenson et al., 1988). Hydrodynamic studies on DAPI–DNA complexes indicate a slight viscosity increase with calf thymus DNA but do not show the sharp viscosity maximum observed for classical intercalation with closed circular superhelical DNA (Manzini et al., 1983). Solution observations have, thus led to an AT-specific, minor groove binding model for the DAPI–DNA complex at low bound ratios of DAPI.

As can be seen in Figure 1, DAPI has the torsional freedom and pattern of hydrogen-bonding N–H groups on the inside face of the molecule typically seen with groove-binding molecules. DAPI can, thus, form hydrogen bonds to thymine O2 and adenine N3 atoms in a minor-groove complex as observed with netropsin and other related molecules (Larsen et al., 1989; Kopka et al., 1985b; Coll et al., 1989; Pjura et al., 1987). Dickerson and co-workers have solved the crystal structure of one DAPI molecule bound to the self-comple-

† This work was supported by Grant NIH-NIAID AI-27196 and by a NSF equipment grant for the Varian VXR 400.

‡ Georgia State University.
§ Emory University.
∥ University of Southampton.

[1] Abbreviations: CT-DNA, calf thymus deoxyribonucleic acid; CD, circular dichroism; DAPI, 4'6-diamidino-2-phenylindole; DNA, deoxyribonucleic acid; EDTA, ethylenediaminetetraacetic acid; MES, 2-(*N*-morpholino)ethanesulfonic acid; poly[d(A-T)]$_2$, poly[d(A-T)]·poly[d(A-T)]; poly[d(G-C)]$_2$, poly[d(G-C)]·poly[d(G-C)]; TSP, 3-(trimethylsilyl)propionic acid; SDS, sodium dodecyl sulfate.

0006-2960/90/0429-8452$02.50/0

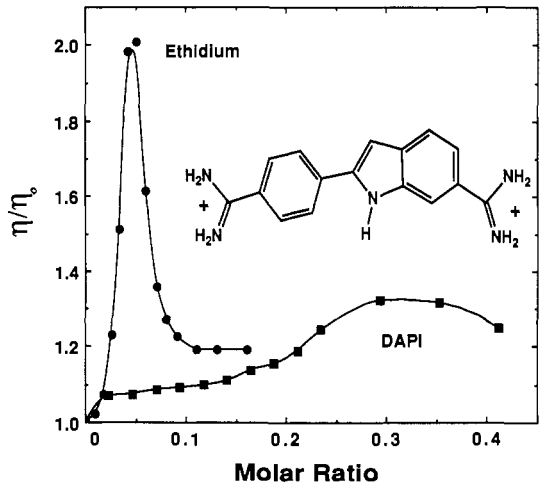

FIGURE 1: Viscometric titrations of closed circular supercoiled DNA with ethidium (●) and DAPI (■). Structure of DAPI is shown above the plot. The reduced specific viscosity ratio is plotted as a function of molar ratio of compound to DNA base pairs. Experiments were conducted in MES buffer at 30 °C.

mentary duplex of d(CGCGAATTCGCG), and as with netropsin, DAPI binds in the AATT central region of the oligomer minor groove (Kopka et al., 1985a,b,c; Larsen et al., 1989). It is thus clear that DAPI forms a selective complex in sequences of three to four AT base pairs which is quite favorable and is stabilized by the molecular electrostatic potential of the minor groove in AT sequences (Pullman & Pullman, 1981), hydrogen bonding, and van der Waals interactions.

As a result of an extensive series of studies with unfused aromatic cations as bleomycin amplifiers, we have found that such compounds, which are similar in structure to unfused aromatic groove-binding molecules such as DAPI, can bind to DNA by intercalation (Wilson et al., 1988, 1989b; Strekowski et al., 1987). This observation suggested that DAPI, and perhaps other groove-binding molecules, might bind to GC-rich regions of DNA by intercalation. Preliminary studies with poly[d(G-C)]$_2$ clearly demonstrated that DAPI binds strongly to the polymer and that the preferred DAPI binding mode at GC base pairs is intercalation (Wilson et al., 1989a, 1990). DAPI thus presents a valuable experimental model system for exploration of the molecular basis of base-pair and binding-mode specificity. We report here a detailed comparison of its interactions with poly[d(A-T)]$_2$ and poly[d(G-C)]$_2$. These studies are particularly relevant considering the intense efforts currently underway to design DNA binding agents which show base pair specific interactions.

Materials and Methods

Materials. DAPI was obtained from Boehringer Mannheim Biochemicals. No impurities could be detected in its high-resolution NMR spectra. MES buffer contained 0.01 M MES and 1×10^{-3} M EDTA. Sodium chloride was added to obtain the desired salt concentration, and the buffer pH was adjusted to 6.2 with NaOH. Poly[d(G-C)]$_2$, poly[d(A-T)]$_2$, and poly(dA)·poly(dT) were purchased from P-L Biochemicals. Poly[d(G-C)]$_2$ and poly[d(A-T)]$_2$ were sonicated, purified, and dialyzed against MES buffer for the NMR study as previously described (Wilson et al., 1985a,b). CT-DNA and closed circular supercoiled DNA were prepared as previously described (Wilson et al., 1988).

Linear Dichroism. Linear dichroism experiments were conducted as previously described (Banville et al., 1985, 1986). Solutions were prepared with gentle stirring by adding ligand to an unsonicated CT DNA (7.7 mM) solution in MES buffer with added 0.1 M NaCl. Data were obtained by recording the absorbance before, during, and after flow. Only the results in which the absorbance was the same before and after the flow were used in the calculations. To determine the absorbance of solutions without flow, an aliquot of solution was diluted with MES buffer without NaCl, which was used to ensure minimal dissociation of the ligand from DNA, and the absorbance was determined at 260 nm and the complex maximum absorbance wavelength above 300 nm.

Viscometric Titrations. Viscometric titrations were conducted as previously described (Jones et al., 1980) in MES buffer at 30 °C. Details of the experimental conditions are given in the figure legends.

Spectrophotometric Measurements. Scans, extinction coefficients, and equilibrium constants were determined as previously described (Wilson et al., 1985a; Wilson & Lopp 1979) with either a Cary 2200 or a Cary 219 spectrophotometer.

Equilibrium Dialysis. Poly[d(A-T)]$_2$ solutions (3×10^{-6} M in base pairs, 3 mL in each cell) were dialyzed against buffer containing different concentrations of DAPI in Plexiglas equilibrium dialysis cells as previously described (Strickland et al., 1988). Spectra/Por dialysis membrane (Spectrum Medical Industries, Inc.) were used, and equilibrium was reached within 15 days with little binding of DAPI to the membrane. The concentration of free DAPI in the dialyzate was measured directly from the fluorescence intensity with reference to a standard curve prepared from DAPI solutions of known concentrations. The amount of total DAPI in the DNA cell was determined by adding an aliquot to a 1% of SDS solution in MES buffer. Control experiments indicated no binding of DAPI to DNA under these conditions. The total DAPI concentration could then be determined from a standard fluorescence curve in the SDS solution.

Circular Dichroism. CD spectra were obtained on a Jasco J-600 spectrometer interfaced to an IBM-PC computer. The software supplied by Jasco provided instrument control, data acquisition, and manipulation. Solutions of DAPI in MES buffer at 25 °C were scanned in 1-cm quartz cuvettes. Concentrated solutions of the polymer were added, and the sample was rescanned at all desired ratios.

DNA Footprinting. The 160 base pair TyrT DNA fragment was isolated and labeled at the 3′-end of the *Eco*RI site with reverse transcriptase and [a-^{32}P]dATP. DNase I footprinting were performed as previously described (Fox & Waring, 1984). The products of digestion were resolved on 8% polyacrylamide gels containing 8 M urea. Gels were fixed in acetic acid, dried under vacuum at 80 °C, and exposed to autoradiography at −70 °C with an intensifying screen. Bands in the digests were assigned by comparison with Maxam–Gilbert dimethyl sulfate–piperidine markers specific for guanine. Autoradiographs were scanned on a Joyce-Loeble Chromoscan 3 microdensitometer. From these data differential cleavage plots were calculated as previously described (Fox & Waring, 1984) so that negative values indicate drug-induced protection from cleavage; positive values indicate enhanced cleavage. In several places the intensity of bands in the DAPI-treated lanes is too small to measure accurately because of the large protection afforded by the ligand. These areas are indicated by the hatched bars in Figure 2B.

NMR. Spectra of solutions of DAPI were obtained as previously described (Chandrasekaran et al., 1986; Wilson et al., 1985c) in a D_2O buffer (0.01 M MES, 0.01 M EDTA, 0.1 M NaCl, pH 6.2) at high temperature (50–80 °C) and

low enough concentration (0.5 mM or less) so that no concentration-induced shifts were observed. Sonicated DNA polymer samples (~200 base pairs) were added and the shifts again determined. Spectra were collected on a Varian VXR 400 spectrometer at a spectral width of 4500 Hz, with 10000 data points, a 1-s relaxation delay, typically 128 transients, and TSP as an internal reference.

Kinetics. Kinetic measurements were conducted with a Hi-Tech SF-51 stopped-flow spectrometer. The HS-1 Datapro software provided with the instrument was used for both data acquisition and analysis. The data acquisition was carried out via a high-speed (>80 kHz) 12-bit analogue to digital convertor mounted in a HP-330 computer interfaced to the SF-51 stopped-flow spectrometer. Single-wavelength kinetic records of voltage versus time were collected and converted to absorbance. Typically 5–10 runs were collected and averaged by the computer to improve the signal to noise ratio. Dissociation reactions were monitored by mixing equal volumes (100 μL) of a DNA–drug complex with a 1% solution of SDS at the same salt concentration. The temperature was controlled by a Haake A81 refrigerated water bath.

DNA Degradation by Bleomycin. The effect of DAPI on belomycin-mediated degradation of poly[d(A-T)]$_2$ and poly-[d(G-C)]$_2$ in the presence of ferrous ion and dithiothreitol (an iron reducing agent) was measured by HPLC analysis of the DNA bases released during the degradation as described previously (Strekowski et al., 1989).

Results

Viscometric Titrations and Linear Dichroism. Titrations of closed circular Col E$_1$ DNA with ethidium and DAPI are compared in Figure 1. Ethidium gives the unwinding viscosity maximum at the open circular state and rewinding with viscosity decrease expected of a classical intercalator. The DAPI viscometric titration also suggests DNA intercalation; however, the viscosity maximum is broader and shifted to higher ratios as expected if intercalation occurs only at selected sequences in the DNA.

The linear dichroism of flow-oriented complexes of calf thymus DNA was determined, and reduced dichroism (^{red}D) results were calculated:

$$^{red}D = (A_{\parallel} - A_{\perp})/A_0 \qquad (1)$$

where $A_{\parallel} - A_{\perp}$ is the difference in absorbance for light polarized parallel and perpendicular to the direction of flow and A_0 is the absorbance of the stationary sample. Complexes of DAPI with high molecular weight CT-DNA have negative linear dichroism at 260 nm ($^{red}D = -0.170$) as expected for the DNA bases in a B-form duplex. At the DAPI maximum wavelength in the complex (340 nm) however, the ^{red}D is positive ($^{red}D = +0.056$), at low ratios of DAPI per base pair, indicating a strong binding mode with an orientation of DAPI more parallel then perpendicular to the helix axis. Hoechst 33258 ($^{red}D = +0.078$) and distamycin ($^{red}D = +0.110$) have similar reduced dichroism values at the complex maximum wavelength, but the dicationic intercalator propidium has an opposite reduced dichroism ($^{red}D = -0.170$). As the ratio of DAPI per base pair is increased, the reduced dichroism of its complex decreases.

DNA Footprinting. Figure 2A presents gel results for DNase I footprinting of the tyrT DNA fragment in the presence and absence of distamycin and DAPI, and Figure 2B is a differential cleavage plot for the 1 μM DAPI results in Figure 2A. At low concentrations both ligands produce clear footprints which are found at AT-rich regions. These

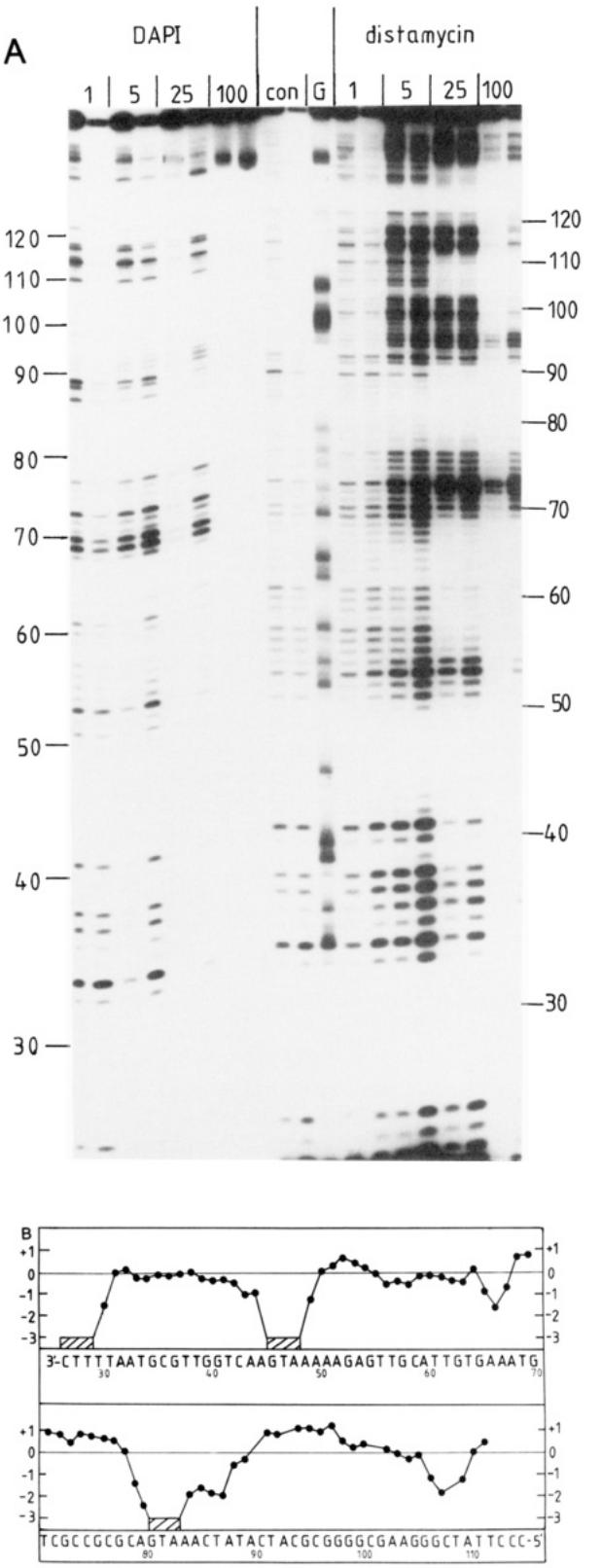

FIGURE 2: (A) DNase I footprinting of the 160 base pair tyrT DNA fragment in the absence (con) and presence of DAPI and distamycin. The DNA was labeled at the 3′-end of the *Eco*RI site. Drug concentations (μM) are indicated at the top of the lanes. Each pair of lanes corresponds to digestion by the enzyme for 1 and 5 min. The track labeled "G" is a Maxam–Gilbert dimethyl sulfate–piperidine marker specific for guanine. Numbers correspond to the sequence shown in Figure 4B. (B) A differential cleavage diagram for the results in Figure 4A. Only the relevant portion of the sequence is shown. The hatched areas correspond to regions where the intensity of bands in the DAPI-treated lanes was too small to measure.

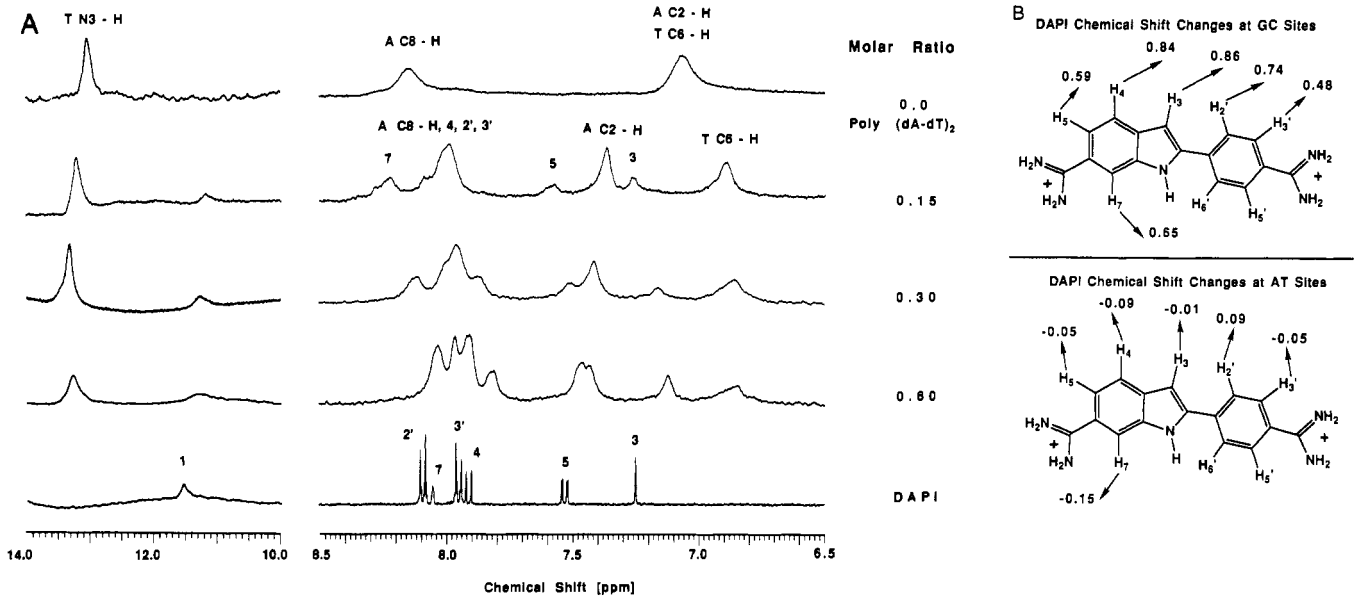

FIGURE 5: (A) ^{1}H NMR titrations of (right side) the aromatic proton region of DAPI with sonicated poly[d(A-T)]$_2$ at 60 °C in D_2O and (left side) the imino proton region of sonicated poly[d(A-T)]$_2$ with DAPI at 30 °C in H_2O/D_2O. The molar ratio of DAPI to base pairs is shown in the figure. Spectra were collected on a Varian VXR 400-MHz spectrometer in MES buffer with 0.1 M NaCl. Assignments in the figure were made with standard COSY and NOESY 2D methods. (B) Schematic plots of the DAPI aromatic proton signal chemical shift changes at GC sites and at AT sites at a ratio of 0.15 DAPI/base pair.

can most clearly be seen in the gel results around positions 66, 82, and 110. Other protections at positions 28, 45, and 125 are less clear since the enzyme has a very low rate of cleavage at these positions in the control. At all concentrations distamycin induces enhanced rates of DNase I cleavage in certain GC-rich regions (around 75, 95, and 115). These have previously been interpreted as arising from drug-induced changes in DNA structure rendering the DNA more susceptible to DNase I attack (Fox & Waring, 1984). No such enhancements are visible with DAPI at all concentrations; this ligand is clearly affecting DNA structure differently than distamycin.

As can be seen in Figure 2B, all of the protections at low concentration are found toward the 3'-end of runs of A and T as expected for footprinting of an AT-specific ligand, since DNase I cuts across the minor groove for which the closest phosphates are staggered two to three bases in the 3' direction. Protection at each site is not identical so that the long block between 80 and 90, which consists of two runs of four AT base pairs, is protected at AAAT better than at ATAT. Generally, the best protections at low ratio seem to be in homopolymeric regions of A or T. It is interesting to note that TTA at position 60 is not significantly protected. At the highest concentrations DAPI completely abolishes DNase I cleavage. It appears that the ligand is bound to many sites along the DNA helix and that these are at both GC and AT sites.

We have also performed footprinting experiments using micrococcal nuclease (MNase) as the probe (data not shown). This enzyme is especially useful since it cuts exclusively at pA and pT bonds. At low concentrations both ligands produce large protections from MNase attack, similar to those previously reported (Fox & Waring, 1987; Portugal & Waring, 1988). However, at the highest concentration (100 μM) of DAPI an MNase cleavage pattern is restored which is similar to, but not identical with, that of the control. No such changes are produced by distamycin.

Absorption and Circular Dichroism Spectra. Both polymer samples cause decreases in the DAPI extinction coefficient and shifts of the absorption maximum to longer wavelength [Figure 3; see supplementary material (see paragraph at end of paper regarding supplementary material)]. Under similar conditions, greater extinction coefficient decreases are seen with poly[d-(G-C)]$_2$ than with poly[d(A-T)]$_2$.

Free DAPI has no intrinsic CD; however, binding of DAPI to DNA results in an induced CD spectrum. CD spectra in the presence of poly[d(A-T)]$_2$ and poly[d(G-C)]$_2$ are quite different (Figure 4; see supplementary material). Titration of DAPI with poly[d(A-T)]$_2$ results in a CD curve with a peak at approximately 370 nm and a shoulder at lower wavelength at ratios of >0.30 (Figure 4A). At ratios less than 0.30, a peak appears in the 330–340-nm region, and the signal at 370 nm decreases. Initial addition of the GC polymer to DAPI results in a CD signal at 350–360 nm. Continued addition of the polymer causes a decrease in intensity and a shift of the CD band to lower wavelength. The induced CD intensity of the AT polymer complex is greater than that for the GC complex.

NMR. Most of the aromatic proton signals for DAPI and DNA are resolved and can be monitored on complex formation. Imino proton signals for the AT and GC polymers can be monitored in H_2O and suggest significantly different interactions of DAPI with the base pairs in these two different DNA sequences: the T imino proton signal of poly[d(A-T)]$_2$ shifts downfield (Figure 5A) and the G imino peak of poly-[d(G-C)]$_2$ shifts upfield (Wilson et al., 1989a, 1990) on complex formation with DAPI. Phosphorus NMR signals of the polymers (not shown) also shift in opposite directions on addition of DAPI: the poly[d(A-T)]$_2$ signal shifts upfield, and the poly[d(G-C)]$_2$ ^{31}P signal shifts downfield.

All DAPI aromatic protons shift significantly upfield at all ratios in the presence of poly[d(G-C)]$_2$ (Figure 5B), and the G and C base aromatic protons also shift slightly upfield on titration of the polymer with DAPI (Wilson et al., 1989a). In free poly[d(G-C)]$_2$ the H1' proton signals of G and C overlap at 5.7 ppm. On addition of DAPI to a 0.3 ratio, they are slightly resolved as the GH1' signal shifts ~0.03 downfield and the CH1' signal shifts ~0.02 upfield. With poly[d(A-T)]$_2$ there are three base aromatic protons, AH8, AH2, and TH6, and their shift changes on addition of DAPI are quite large and different than those with poly[d(G-C)]$_2$. In the free polymer the AH2 and the TH6 signals overlap at 7.07 ppm,

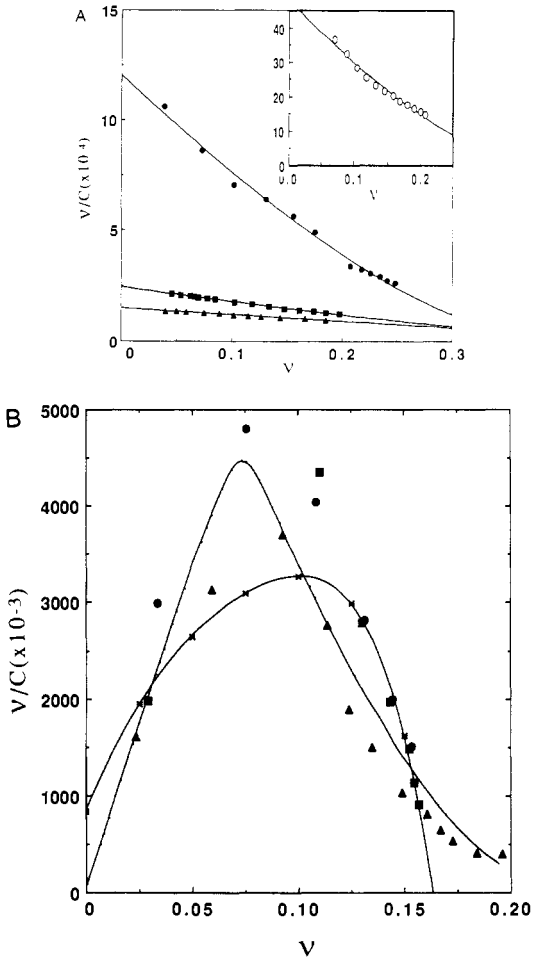

FIGURE 6: Scatchard plots for binding of DAPI to (A) poly[d(G-C)]$_2$ and (B) poly[d(A-T)]$_2$. (A) Experiments were at 25 °C in MES buffer at different ionic strengths: (○) 0.05 M NaCl, (●) 0.10 M NaCl, (■) 0.20 M NaCl, and (▲) 0.30 M NaCl. Points in the figure are the experimental results, and the solid lines are the best fits from the McGhee–von Hippel site-exclusion model. (B) Experiments were at 25 °C in MES buffer with 0.30 M NaCl added. Points in the figure are the experimental data. The solid line is the best fit from the Crother's allosteric model, and the line marked by × is the fit with the McGhee–von Hippel model. The allosteric model parameters are $K_1 = 9.3 \times 10^4$, $K_2 = 8.4 \times 10^6$, $n_1 = 4$, $n_2 = 4$, $\sigma = 0.002$, and $s = 0.91$.

and the AH8 signal is at 8.15 ppm. On addition of excess DAPI to the polymer (0.6 ratio in Figure 5A), both major-groove protons, TH6 and AH8, move approximately 0.2 ppm upfield while the minor-groove proton, AH2, moves downfield approximately 0.35 ppm. The H1′ protons of A and T in poly[d(A-T)]$_2$ shift significantly upfield on addition of DAPI. Initially, TH1′ is at 6.15 ppm and AH1′ is at 5.14 ppm. Both broaden and shift upfield 0.4–0.5 ppm in the presence of excess DAPI as expected for a minor-groove complex.

The DAPI aromatic protons display unusual behavior on addition of poly[d(A-T)]$_2$. At high ratios of DAPI to polymer bases, the DAPI protons first shift slightly upfield (Figure 5A). On continued addition of poly[d(A-T)]$_2$, the signals shift downfield, and with excess polymer, most of the aromatic proton signals of DAPI are downfield of their original chemical shift positions in unbound DAPI. In contrast, the DAPI aromatic protons shift significantly upfield (0.5–0.9 ppm) on addition of excess poly[d(G-C)]$_2$ (Figure 5B).

The DAPI indole-NH proton, which is observable in H_2O buffer, shifts upfield approximately 0.3 ppm on addition of excess poly[d(A-T)]$_2$ (Figure 5). The proton can be observed only at low temperature in the absence of the polymer but can

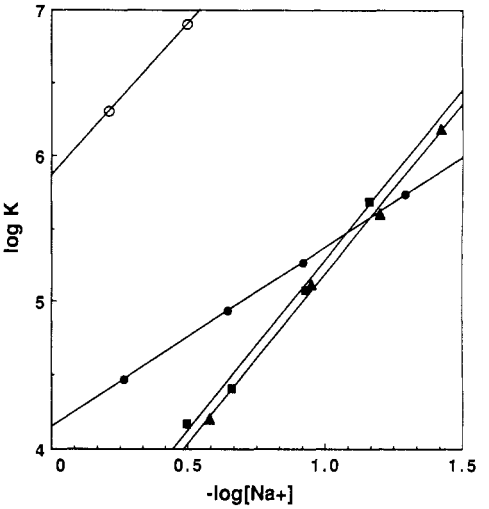

FIGURE 7: Plots of log K, the observed equilibrium constants, determined as in Figure 6 vs −log [Na$^+$]: DAPI/poly[d(G-C)]$_2$ (■), DAPI/poly[d(A-T)]$_2$ (○), ethidium/CTDNA (●), and quinacrine/CTDNA (▲). The solid lines are linear least-squares best-fit values. Ethidium and quinacrine have very similar plots for the AT and GC polymers as with CT-DNA. Because of the very strong, highly cooperative binding of DAPI to the AT polymer, K values could be obtained at only two salt concentrations.

be seen at higher temperatures in the complexes. The indole N–H is broader and is shifted farther upfield when DAPI is bound to poly[d(G-C)]$_2$ than when bound to poly[d(A-T)]$_2$.

Binding Studies. Binding isotherms for DAPI with poly[d(A-T)]$_2$ and poly[d(G-C)]$_2$ are both qualitatively and quantitatively different (Figure 6). Binding curves with poly[d(G-C)]$_2$ (Figure 6A) are typical of DNA intercalating ligands (Wilson et al., 1989a) and are well fitted with the site-exclusion model of McGhee and von Hippel (1974) (Figure 6A). The observed equilibrium constant (K) decreases with increasing salt concentration, and the slope of a log K versus −log [Na$^+$] plot (Figure 7) is 2.3 in agreement with predictions from the ion-condensation theory for polyelectrolytes (Manning, 1978; Record et al., 1976, 1978; Wilson et al., 1985a). As can be seen in Figure 7, the dicationic intercalator quinacrine has a slope similar to that for the DAPI–GC polymer complex. The results for ethidium, which has only a single charged group, yield a slope of 1.2. Because of their differences in slope, ethidium binds more weakly than DAPI at low salt concentration but more strongly at high salt concentration.

Binding of DAPI to poly[d(A-T)]$_2$ is complex and much stronger than that to poly[d(G-C)]$_2$ under all conditions where measurements could be made. Binding measurements with the AT polymer were made both by absorption spectral changes and by equilibrium dialysis, and the two methods give results that agree quite well considering the difficulty of measuring binding densities for this complex and very strong binding equilibrium (Figure 6B). The interaction of DAPI with poly[d(A-T)]$_2$ displays pronounced positive cooperativity (Figure 6B), and the results cannot be adequately fitted with the model of McGhee and von Hippel (1974). The results are, however, well fitted with the allosteric-transition model of Crothers and co-workers (Hogan et al., 1979; Dattagupta et al., 1980). The experimental binding isotherms were fitted to the allosteric model with a VAX Fortran computer program developed and supplied by Professor Crothers. Briefly, this model describes the ligand binding induced allosteric transition betweeen two forms of DNA. Each base pair exists in one of two forms, labeled 1 or 2, with an equilibrium constant, s, for the conversion between the two forms. The equilibrium

constant describing the initiation of one base pair of form 2 in a form 1 sequence is $\sigma^2 s$, where σ is a cooperativity parameter. The ligand has different affinities (K_1 and K_2) for the two forms. The number of base pairs excluded by a bound ligand in forms 1 and 2 is n_1 and n_2, respectively. The parameter σ is 1.0 for noncooperative binding.

The DAPI–AT results were analyzed with the allosteric model by first fitting the data beyond the ν value corresponding to the maximum in ν/C with the McGhee and von Hippel (1974) neighbor-exclusion model. This fit of the high ν value results provides estimates for K_2 and n_2. Extrapolation of the data at very low ν values to the ν/C intercept allows an estimate of K_1 and n_1. The model thus has six adjustble parameters, K_1, K_2, n_1, n_2, σ, and s, to define the allosteric binding isotherm, and fitting of this model to the experimental results involves an iterative process of varying σ, s, the ratio of K_2/K_1, n_1, and n_2. The parameters s and K_2/K_1 determine the ν value at the maximum ν/C in the isotherm, and σ is related to the degree of cooperativity, the steepness of the isotherm, for the conversion from form 1 to form 2. Values for the six adjustable parameters for the DAPI–poly[d(A-T)]$_2$ binding results are given in Figure 6. The number of base pairs per binding site is four for each conformation, and K_2, for DAPI binding to the second conformation (form 2), is ~90 times larger than K_1.

For qualitative comparisons, log K_2 for DAPI binding to the AT polymer is plotted at two salt concentrations in Figure 7. Binding at lower salt concentrations becomes too strong to measure accurately, and erratic results were obtained at very high salt concentrations. It is obvious, however, that the slope is near 2 for the DAPI–AT complex as with the GC polymer. The AT binding constants, however, are approximately a factor of 1000 larger than the binding constants for the GC polymer (Figure 7).

Binding of DAPI to the mixed base pair, alternating polymer poly[d(A-C)]·poly]d(G-T)] was also determined in MES buffer with 0.1 M NaCl. the shape of the Scatchard plot is similar to that of the plot for DAPI binding to poly[d(G-C)]$_2$, and the results are well fitted with the site-exclustion model ($K = 1.2 \times 10^5$ M^{-1}; two base pairs per binding site). These results are very similar to the values for DAPI binding to poly[d(G-C)]$_2$ and are quite different from the DAPI binding results with poly[d(A-T)]$_2$. Clearly more than one AT base pair is necessary for the very strong and highly cooperative minor-groove binding of DAPI.

Dissociation Kinetics: Effects of Base-Pair Type and Salt Concentration. The DAPI spectral changes on binding to the DNA polymers can also be used to monitor the kinetics of binding. Association reactions of DAPI with AT and GC polymers are too fast to measure by stopped-flow techniques at the lowest possible temperatures and concentrations. The dissociation reactions are much slower, as expected for ligands that bind strongly to DNA, and results for the SDS-driven dissociation of DAPI from poly[d(A-T)]$_2$ and poly[d(G-C)]$_2$ are shown in Figure 8. Two-exponential fits to the data are also shown in the figure with plots of residuals. Single-exponential fits gave unsatisfactory residuals and higher RMS deviations than the two-exponential fits. Three-exponential fits did not significantly improve the residuals or RMS deviations.

With poly[d(A-T)]$_2$ the amplitude for the fast phase of the reaction accounts for ~30% of the total amplitude under all conditions used. With poly[d(G-C)]$_2$ the fast-phase amplitude varied from 45% of the total at low temperature to 85% at high temperature. For the purposes of a comparison, the dissocation

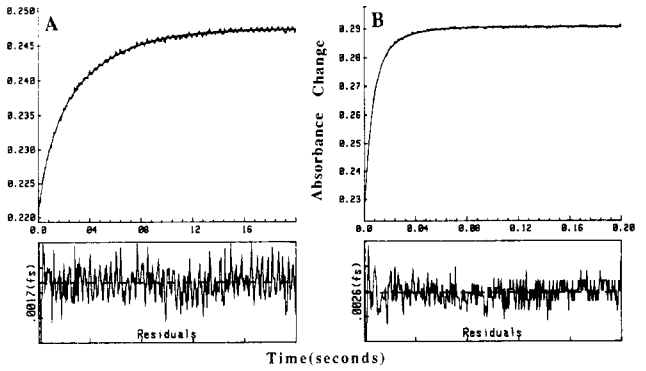

FIGURE 8: Stopped-flow kinetic traces for the SDS-driven dissociation of DAPI from poly[d(A-T)]$_2$ (A) and poly[d(G-C)]$_2$ (B). The experiments were conducted at 20 °C in MES buffer at a ratio of 1:10 DAPI:polymer base pairs. The concentration of DAPI after mixing was 1.25×10^{-5} M. The smooth lines in the panels are the two-exponential fits to the experimental data. Residuals plots for both data sets are shown under the experimental plots.

Table I: Salt Concentration and DNA Polymer Dependence of DAPI Dissociation

[Na$^+$] (M)	k_1 (s^{-1})	% A$_1$	k_2 (s^{-1})	% A$_2$	τ (s)
		Poly[d(A-T)]$_2$[a]			
0.035	1.25	30	0.265	70	1.784
0.085	7.67	17	1.49	83	0.394
0.135	15.6	25	3.59	75	0.152
0.235	38.2	25	8.15	75	0.064
		Poly[d(G-C)]$_2$[b]			
0.035	87.5	70.5	25.3	29.5	0.0145
0.055	160	74.6	51.3	25.4	0.0076
0.085	227	81.8	69.7	18.2	0.0050
0.135	292	84.6	78.3	15.4	0.0038

[a] All experiments were conducted in MES buffer at 20 °C by mixing equal volumes of the DAPI–polymer complex with 1% SDS in the same salt concentration. The [Na$^+$] concentrations are after mixing the complex in buffer with SDS in the same buffer. The ratio of DAPI/DNA in the complex is 1:10 in base pairs. [b] Experiments were conducted at 15 °C.

lifetime (τ) and apparent rate constant ($k_{app} = 1/\tau$) were calculated from the computer-derived, best-fit values for rate constants and amplitudes as suggested by Denny and Wakelin (1985):

$$\tau = 1/(A_1k_1 + A_2k_2) \quad (2)$$

where A and k values refer to the amplitudes and rate constants for the two-exponential fits to the dissociation results (Table I). The amplitudes and rate constants in the two-exponential fits are correlated and are thus quite sensitive to the experimental noise and baseline. This is not true of the apparent rate constants calculated from eq 2.

Kinetics experiments were conducted at constant temperature as a function of salt concentration, and plots of log k_{app} as a function of log [Na$^+$] are shown in Figure 9. Again, quite different results are obtained with the AT and GC polymers. For the SDS-driven dissociation of DAPI from poly[d(G-C)]$_2$ the slope in Figure 9 is 0.8 ± 0.1, and with poly[d(A-T)]$_2$ a slope of 1.8 ± 0.1 is obtained. For comparative purposes the dissociation constants of the dicationic intercalator propidium are also plotted in Figure 9. Propidium intercalates at both AT and GC sequences, and the slopes for dissociation of both complexes are ~0.8. It is quite clear from these results that binding of DAPI to AT and GC sites follows different mechanisms.

Bleomycin Cleavage of DNA: A Probe for Major- versus Minor-Groove Binding. In the presence of Fe(II) bleomycin

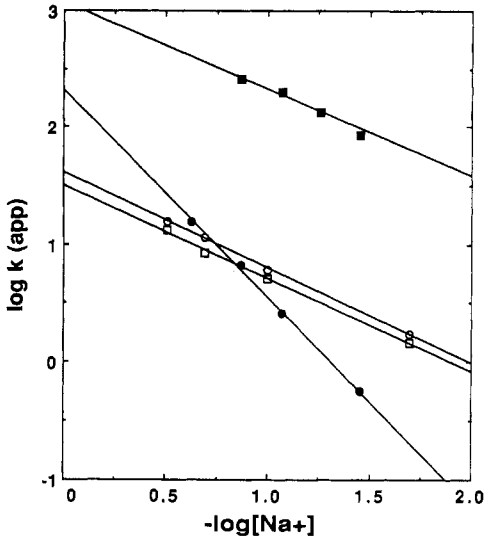

FIGURE 9: Plots of log k_{app} vs $-\log [Na^+]$ for dissociation of DAPI from poly[d(A-T)]$_2$ (●) and from poly[d(G-C)]$_2$ (■) and dissociation of propidium from poly[d(A-T)]$_2$ (○) and from poly[d(G-C)]$_2$ (□). Experiments were conducted in MES buffer at different ionic strengths in the manner described in Figure 8. The propidium results are from Wilson et al. (1985b, 1986).

catalyzes cleavage of the DNA backbone. Some unfused intercalators, which have substituents in the major but not in the minor groove, can enhance this cleavage rate at all ratios (Strekowski et al., 1987). Molecules, such as ethidium, which have substituents in the minor groove cause an enhancement in the catalytic rate at low ratios of compound to DNA but interfere with bleomycin binding at higher ratios and become inhibitors (Bearden & Haidle, 1975; Agostino et al., 1984).

The bleomycin-catalyzed cleavage of poly[d(A-T)]$_2$ and poly[d(G-C)]$_2$ was monitored in the presence of varying concentrations of DAPI by an HPLC method to detect DNA bases liberated in the reaction. With poly[d(A-T)]$_2$ there is an initial slight enhancement of the bleomycin activity which is followed by strong inhibition at higher ratios (not shown). The bleomycin-catalyzed cleavage of the DAPI complex with poly[d(G-C)]$_2$ is markedly enhanced relative to that of the free polymer at all ratios. These results support the minor groove binding mode of DAPI in AT sequences and provide the important result that DAPI is oriented toward the major groove in its GC intercalation complex.

Discussion

All of the results presented here clearly demonstrate that DAPI binds to both AT and GC or mixed regions of DNA but that the complexes formed at these different sequences are qualitatively and quantitatively different. Numerous studies have shown that DAPI binds strongly to the minor groove in DNA sequences containing three to four adjacent AT base pairs (Zimmer & Wahnert, 1986; Dervan, 1986; Pullman & Pullman, 1981; Kapuscinski & Szer, 1979; Manzini et al., 1984; Kubista et al., 1987: Portugal & Waring, 1988). Our linear dichroism and footprinting results at low ratios with natural DNA samples are in complete agreement with these earlier studies, but they also show that, as the ratio of DAPI to DNA base pairs is increased, DAPI binds at GC-containing sites. The unwinding results with supercoiled DNA suggest that the DAPI binding mode at GC and mixed sites is by intercalation. The size and complexity of natural DNA samples precludes a high-resolution analysis of the complex array of DAPI interactions, and to simplify the quantitative comparisons of the AT and GC binding modes of DAPI, we have focused on DNA polymers containing either AT or GC base pairs.

Binding of DAPI to the polymers is characterized by quite different binding isotherms (Figure 6): DAPI binding to poly[d(A-T)]$_2$ is very strong and highly cooperative while binding to poly[d(G-C)]$_2$ follows a simpler site-exclusion model. The strong binding of DAPI to AT base pair sequences was expected, but the cooperative binding was not. The allosteric model for DAPI binding to AT site suggests that the initial binding of the molecule in the minor groove of AT DNA sequences (K_1 in Figure 6A) converts local regions of AT sequences into a conformation (form 2) which binds DAPI much more strongly than the initial DNA conformation. This could occur if, as suggested by the crystallograplhic results of Dickerson and co-workers (Larsen et al., 1989), the minor groove in extended AT sequences is intrinsically too narrow to accept binding of an aromatic system. Initial binding of DAPI in such sequences would thus be energeticaly less favorable than subsequent binding due to the free energy cost of local widening of the groove. Subsequent binding of DAPI could occur by extending this locally widened minor groove (K_2 in Figure 6A). Fitting of the allosteric model to the AT binding results suggests that $K_2/K_1 \sim 90$ or that 2–3 kcal/mol of free energy is required to induce the DNA conformational change from form 1 to form 2 DNA.

Quantitative comparisons of binding constants are informative, and several important features of the DAPI–DNA interactions can be seen from the plot in Figure 7. First, the slopes of plots for both AT and GC binding are approximately 2, indicating that, although the AT and GC complexes are quite different, they both involve two charge interactions with DNA (e.g., two phosphate groups are effectively neutralized by DAPI binding at either AT or GC sites). Second, binding of DAPI to these AT sites is at least a factor of 1000 stronger than binding to the GC sites. It should be emphasized that the DAPI preference for AT sites occurs because binding of DAPI in AT regions is very strong not because binding at GC sites is weak. Comparisons with DNA binding constants for standard intercalators emphasizes this point. The dicationic acridine intercalator quinacrine, for example, has the same slope as and very similar binding constants to DAPI (Figure 7). The monocation ethidium has a slope of approximately 1, as expected, and binds more weakly than DAPI at low salt concentration but more strongly than the DAPI–GC interaction at high salt concentration (Figure 7).

The K_1 value for allosteric binding of DAPI is difficult to determine accurately due to the low DAPI concentrations required but is ~ 90 times less than K_2. The DAPI–GC binding constant is ~ 1000 times less than K_2 (Figure 7), and thus, DAPI is AT specific irrespective of the local AT conformation. AT sequences can vary in their local minor groove width, and this may account for the variation in protection efficiency observed in different AT regions in DNase I footprinting experiments (Figure 2A,B). DAPI has very similar binding isotherms with poly[d(G-C)]$_2$ and poly[dA-C)]·poly[d(G-T)], and there are two important conclusions from this observation: (i) The strong minor groove binding mode of DAPI cannot occur if the AT base pairs are interrupted by GC base pairs, and (ii) the intercalation binding of DAPI, as with most simple intercalators, has little base-pair specificity since G-C and A-C sequences have similar binding constants. It is clear from these binding results that, due to the considerably larger number of GC and mixed sites relative to sites with three or more AT base pairs in natural DNA samples, at relatively moderate ratios of DAPI to DNA base pairs, sites

Scheme I: Limiting Mechanisms: DNA Interaction[a]

Ψ = fraction of counterion (M^+) thermodynamically associated per phosphate

$\Psi = \Psi_c + \Psi_s = 0.88$ $\Psi_c = 0.76$ $\Psi_s = 0.12$

k_a = observed association rate constant

k_d = observed dissociation rate constant

Z = charge of ligand, L

Intercalation: Preequilibrium with a Stable Intermediate

$L + DNA \longleftrightarrow I + n\Psi M^+$ (preequilibrium)

$DNA \longrightarrow Site$ (rate determining step)

$I + Site \longrightarrow C + (Z - n)\Psi M^+$ (observed)

$\delta(\log k_a)/\delta(\log[M^+]) = -n\Psi \sim -0.7\,Z$

$\delta(\log k_d)/\delta(\log[M^+]) = (Z - n)\Psi \sim 0.24 + 0.16\,Z$

Groove-Binding: Screening Controlled Association

$L + Site \longrightarrow C_1 + x\Psi M^+$ (observed)

$C_1 \longrightarrow C_2 + (Z - x)\Psi M^+$ (final complex)

$\delta(\log k_a)/\delta(\log[M^+]) = -Z\Psi_s \sim -0.12\,Z$

$\delta(\log k_d)/\delta(\log[M^+]) = Z\Psi_c \sim 0.76\,Z$

[a] For references, see Lohman et al. (1978), Lohman (1985), and Wilson et al. (1985a).

containing GC base pairs will be appreciably populated with DAPI. This is consistent with the dramatic change in footprinting results observed on increasing ratios of DAPI.

As with the binding results, the kinetics of dissociation of DAPA from the AT and GC polymers are also strikingly different (Figure 8) and provide important information on the DAPI binding mechanism. As can be seen in Figure 8, under a standard set of conditions, the dissociation of DAPI from an AT complex is ~100 times slower than from a GC complex. The dissociation reactions for complexes with both polymers are biphasic (Table I), perhaps due to the alternating sequence of the polymers (e.g., the base pair at the 5'-end of the complex can be either a purine or a pyrimidine). The biphasic rate constants with both polymers differ by only a factor of ~4, suggesting that the two AT and the two GC rate processes are quite similar and are only distinguishable in the high-resolution kinetics experiments. Such small differences, for example, could not be detected in the lower resolution binding isotherms (cf. Figure 6). Because of the similarity in the biphasic constants and the additional experimental error inherent in fitting two overlapping rate processes, comparisons of DAPI dissociation kinetics with AT and GC polymers have been made with apparent kinetic constants (eq 2).

The effects of salt concentration on dissociation of DAPI from the AT and GC complexes are quite different and, along with NMR results, provide key information to establish the DAPI binding mode. Record and co-workers [cf. Lohman (1985) and Lohman et al., 1978)] have shown that limiting mechanisms for ligand–DNA complex formation can be distinguished by the effects of salt concentration on the rate constants (Scheme I). A screening-controlled, direct-binding process, which, for example, might be viewed as a limiting mechanism for groove-binding molecules, is affected quite differently by salt concentration than binding reactions, such as intercalation, which have stable intermediates formed in a preequilibrium step in the mechanism. These two limiting mechanisms and the effects of salt concentration on their observed association and dissociation constants are outlined in Scheme I. Although association rates were too fast to be monitored for DAPI–DNA complexes, k_d values for both the AT and GC alternating DNA polymers were determined as a function of salt concentration (Figure 9). DAPI dissociation from the AT polymer is approximately twice as sensitive to changes in salt concentration as dissociation from the GC complex, and the slope of the AT plot is in the range predicted for groove interactions of a dication while the GC value is in the intercalation range. The differences in rate constants and slopes for the AT and GC polymers are characteristic of DAPI and not the DNA samples since the nonspecific intercalator propidium has quite similar rates and slopes for complexes with both polymers (Figure 9).

It is interesting that although the DAPI dissociation rate from AT sites is slower than from GC sites, the predicted mechansim, a screening-controlled process, is actually simpler for the AT complex. It should be noted that the rate of the allosteric transition for binding of DAPI to AT sites cannot be the rate-limiting step or a screening-controlled process would not be observed. If the conformational change is a rapid thermal motion that leads to widening of the minor groove in the polymer, it is reasonable that this opening would be a faster process than diffusion of DAPI to the DNA molecule.

The effects of salt concentration of the binding of intercalators, such as propidium, to DNA have previously been investigated in detail (Wilson et al., 1985ab, 1986). As summarized in Scheme I, the mechanism involves a preequilibrium external ionic interaction of the cationic intercalator with DNA. The molecule can then "slide" along the DNA backbone to search for an open intercalation site. Presumably, open sites, satisfactory for intercalation, occur between base pairs as part of the large-amplitude thermal motions of DNA. Formation of the intercalator complex is slower than diffusion of ligands to the DNA molecule and is the rate-determining step in intercalation. The effects of salt concentration are, thus, quite different for the kinetics of dissociation of AT and GC complexes with DAPI and indicate that different mechanisms are involved in AT and GC complex formation, e.g., intercalation at GC sites and groove binding at AT sequences.

The concept of totally different binding modes for DAPI at AT and GC DNA sequences is strongly supported by NMR results with the two alternating polymers (summarized in Figure 5B). In an intercalation complex the local base pair ring current effects cause significant upfield shifts of the intercalator aromatic protons (Wilson & Li, 1990) as observed on formation of the DAPI–GC complex. In a minor-groove complex the contact of bound molecules with the walls of the groove is closer than with the base pairs, and the shifts on complex formation are, thus, less than those observed with intercalation. The edges of the base pairs which face the minor groove would be expected to induce small downfield shifts in the proton signals of molecules which bind in that groove. Thus, small mixed upfield and downfield shifts are observed for DAPI proton signals on formation of the AT complex. In particular, H7, which is on the face of the DAPI molecule near the edges of the bases on the floor of the minor groove, has the largest downfield shift in the AT complex.

Molecular modeling studies which are in progress suggest that the minor-groove complex of DAPI in AT sequences is quite similar to that in the netropsin complex. The intercalation complex is similar to that observed in the X-ray structure of proflavin with dinucleotides (Neidle, 1989) and predicted for other unfused aromatic intercalators (Wilson et al., 1988, 1989b). In the model the DAPI amidine groups project into the major grove in this complex and are sterically prevented from forming an intercalation complex with the amidine groups

in the minor groove. This type of complex structure is supported by the enhancement of bleomycin-catalyzed cleavage of poly[d(G-C)]$_2$ in the presence of DAPI (Strekowski et al., 1989). NMR studies with DNA oligomer complexes of DAPI are in progress to obtain more details of the molecular structure of both binding modes.

ACKNOWLEDGMENTS

We thank Professor Donald Crothers for the program, and instructions for its use, for fitting allosteric binding isotherms. We also thank Professor J. B. Chaires for suggestions on the treatment of allosteric binding results.

SUPPLEMENTARY MATERIAL AVAILABLE

Figure 3 showing spectral shifts of DAPI on titration with poly[d(A-T)]$_2$ and poly[d(G-C)]$_2$ and Figure 4 showing circular dichroism spectra of DAPI with poly[d(A-T)]$_2$ and poly[d(G-C)]$_2$ (5 pages). Ordering information is given on any current masthead page.

REFERENCES

Agostino, M. J., Bemacki, R. J., & Beerman, T. A. (1984) *Biochem. Biophys. Res. Commun. 120*, 156–163.

Banville, D. L., Wilson, W. D., & Marzilli, L. G. (1985) *Inorg. Chem. 24*, 2479–2483.

Banville, D. L., Marzilli, L. G., Strickland, J. A., & Wilson, W. D. (1986) *Biopolymers 25*, 1837–1858.

Bearden, J., Jr., & Haidle, C. W. (1975) *Biochem. Biophys. Res. Commun. 65*, 371–377.

Breslauer, K. J., Remeta, D. P., Chou, W.-Y., Ferrante, R., Curry, J., Zaunczkowski, D., Snyder, J. G., & Marky, L. A. (1987) *Proc. Natl. Acad. Sci. U.S.A. 84*, 8922–8926.

Cavatorta, P., Masotti, L., & Szabo, A. G. (1985) *Biophys. Chem. 22*, 11–16.

Chandresekaran, S., Kusuma, S., Boykin, D. W., & Wilson, W. D. (1986) *Magn. Reson. Chem. 24*, 630–637.

Coll, M., Frederick, C. A., Wang, A. H.-J., & Rick, A. (1987) *Proc. Natl. Acad. Sci. U.S.A. 84*, 8385–8389.

Coll, M., Agmami, J., van der Marel, G. A., van Bloom, J. H., Rich, A., & Wang, A. H.-J. (1989) *Biochemistry 28*, 310–320.

Dattagupta, N., Hogan, M., & Crothers, D. M. (1980) *Biochemistry 19*, 5998–6005.

Denny, W. A., Atwell, G. J., Baguley, B. C., & Wakelin, L. P. G. (1985) *J. Med. Chem. 28*, 1568–1574.

Dervan, P. B. (1986) *Science 232*, 464–471.

Fox, K. R., & Waring, M. J. (1984) *Nucleic Acids Res. 12*, 9271–9285.

Fox, K. R., & Waring, M. J. (1987) *Biochim. Biophys. Acta 909*, 145–155.

Gale, E. F., Cundiffe, E., Reynolds, P. E., Richmond, M. H., & Waring, M. J., Eds. (1981) *The Molecular Basis of Antibiotic Action*, 2nd ed., pp 258–401, Wiley, London.

Hogan, M., Dattagupta, N., & Crothers, D. M. (1979) *Nature 278*, 521–524.

Jones, R. L., Lanier, A. C., Keel, R. A., & Wilson, W. D. (1980) *Nucleic Acids Res. 8*, 1613–1624.

Jorgenson, K. F., Varshney, U., & van de Sande, J. H. (1988) *J. Biomol. Structure Dyn. 5*, 1005–1023.

Kapuscinski, J., & Szer, W. (1979) *Nucleic Acids Res. 6*, 3519–3534.

Kopka, M L., Pjura, P., Yoon, C., Goodsell, D., & Dickerson, R. E. (1985a) in *Structure and Motion: Membranes, Nucleic Acids and Proteins* (Clementi, E., Corongiu, G., Sarma, M. H., & Sarma, R., Eds.) pp 461–483, Adenine Press, New York.

Kopka, M. L., Yoon, C., Goodsell, D., Pjura, P., & Dickerson, R. E. (1985b) *Proc. Natl. Acad. Sci. U.S.A. 82*, 1376–1380.

Kopka, M. L., Yoon, C., Goodsell, D., Pjura, P., & Dickerson, R. E. (1985c) *J. Mol. Biol. 183*, 553–563.

Kubista, M., Akerman, B., & Norden, B. (1987) *Biochemistry 26*, 4545–4553.

Larsen, T. A., Goodsell, D. S., Cascio, D., Grzeskowiak, K., & Dickerson, R. E. (1989) *J. Biomol. Structure Dyn. 7*, 477–491.

Latt, S. A. (1976) *Annu. Rev. Biophys. Bioeng. 5*, 1–37.

Lohman, T. M. (1985) *CRC Crit. Rev. Biochem. 19*, 191–235.

Lohman, T. M., DeHaseth, P. L., & Record, M. T. (1978) *Biophys. Chem. 8*, 281–294.

Manning, G. S. (1978) *Q. Rev. Biophys. 11*, 179–246.

Manzini, G., Barcellona, M. L., Avitabile, M., & Quadrifoglio, F. (1983) *Nucleic Acids Res. 11*, 8861–8876.

McGhee, J. D., & von Hippel, P. H. (1974) *J. Mol. Biol. 86*, 489–489.

Neidle, S. (1989) Landolt-Bornstein, in *Nucleic Acids* (Saenger, W., Ed.) Vol. VII/1b, pp 247–276, Spring-Verlag, Berlin and Heidelberg.

Pjura, P. E., Grzeskowiak, K., & Dickerson, R. E. (1987) *J. Mol. Biol. 197*, 257–271.

Portugal, J., & Waring, M. J. (1988) *Biochim. Biophys. Acta 949*, 158–168.

Pullman, A., & Pullman, B. (1981) *Q. Rev. Biophys. 14*, 289–380.

Record, M. T., Lohman, T. M., & DeHaseth, P. (1976) *J. Mol. Biol. 107*, 145–158.

Record, M. T., Jr., Anderson, C. F., & Lohman, T. M. (1978) *Q. Rev. Biophys. 11*, 103–178.

Strekowski, L., Strekowska, A., Watson, R. A., Tanious, F. T., Nguyen, L. T., & Wilson, W. D. (1987) *J. Med. Chem. 30*, 1415–1420.

Strekowski, L., Mokrosz, J. L., & Wilson, W. D. (1988) *FEBS Lett. 24*, 24–28.

Strekowski, L., Harden, D. B., Wydra, R. L., Stewart, K. D., & Wilson, W. D. (1989) *J. Mol. Recognit. 2*, 158–166.

Strickland, J. A., Marzilli, L. G., Gay, K. M., & Wilson, W. D. (1988) *Biochemistry 27*, 8870–8878.

Wilson, W. D. (1990) in *Nucleic Acids in Chemistry and Biology* (Blackburn, M., & Gait, M., Eds.) Chapter 8, IRL Press Ltd., Oxford, U.K.

Wilson, W. D., & Lopp, I. G. (1979) *Biopolymers 18*, 3025–3041.

Wilson, W. D., & Li, Y. (1990) in *Advances in DNA Sequence Specific Agents* (Hurley, L., Ed.) JAI Press, Greenwich, CT (in press).

Wilson, W. D., Krishnamoorthy, C. R., Wang, Y. H., & Smith, J. C. (1985a) *Biopolymers 24*, 1941–1961.

Wilson, W. D., Wang, Y. H., Krishnamoorthy, C. R., & Smith, J. C. (1985b) *Biochemistry 24*, 3991–3999.

Wilson, W. D., Wang, Y. H., Kusuma, S., Chandrasekaran, S., Yong, N. C., & Boykin, D. W. (1985c) *J. Am. Chem. Soc. 107*, 4989–4995.

Wilson, W. D., Wang, Y. H., Krishnamoorthy, C. R., & Smith, J. C. (1986) *Chem.-Biol. Interact. 58*, 41–57.

Wilson, W. D., Strekowski, L., Tanious, F., Watson, R., Mokrosz, J. L., Strekowska, A., Webster, G., & Neidle, S. (1988) *J. Am. Chem. Soc. 110*, 8292–8299.

Wilson, W. D., Tanious, F. A., Barton, H. J., Strekowski, L., Boykin, D. W., & Jones, R. L. (1989a) *J. Am. Chem. Soc. 111*, 5008–5010.

Wilson, W. D., Tanious, F. A., Watson, R., Barton, H. J., Strekowska, A., Harden, D. B., & Strekowski, L. (1989b) *Biochemistry 28*, 1984–1992.
Wilson, W. D., Tanious, F. A., Barton, H. J., Wydra, R. L., Jones, R. L., Boykin, D. W., & Strekowski, L. (1990) *Anti-Cancer Drug Design. 5*, 31–42.
Zimmer, Ch., & Wahnert, U. (1986) *Prog. Biophys. Mol. Biol. 47*, 31–112.

Effect of the Antitumor Drug *cis*-Diamminedichloroplatinum(II) and Related Platinum Complexes on Eukaryotic DNA Replication†

Wendy J. Heiger-Bernays,‡,§ John M. Essigmann,*,‡,§ and Stephen J. Lippard*,‡
Department of Chemistry and Whitaker College of Health Sciences and Technology, Massachusetts Institute of Technology, Cambridge, Massachusetts 02139
Received April 20, 1990

ABSTRACT: An SV40-based in vitro replication system has been used to examine the effects of platinum compounds on eukaryotic DNA replication. Plasmid templates containing the SV40 origin of replication were modified with the anticancer drug *cis*-diamminedichloroplatinum(II) (*cis*-DDP, cisplatin) or the inactive analogues $[Pt(dien)Cl]^+$ and *trans*-DDP. The platinated plasmids were used as templates for DNA synthesis by the DNA polymerases present in cytosolic extracts prepared from human cell lines HeLa and 293. Bifunctional adducts formed by *cis*- and *trans*-DDP inhibited DNA replication by 95% at a bound drug to nucleotide ratio $[(D/N)_b]$ of $<9 \times 10^{-4}$, in contrast to the monofunctional $[Pt(dien)Cl]^+$ analogues, which required a $(D/N)_b$ of 3.4×10^{-3} for 62% inhibition of DNA replication. An average of two platinum adducts per genome was sufficient for inhibition of DNA replication by cisplatin. When *trans*-DDP-modified, but not *cis*-DDP-modified, SV40 origin containing plasmids $[(D/N)_b = 1.7 \times 10^{-3}]$ were allowed to incubate in the 293 cytosolic extracts for 1 h prior to addition of T-antigen to initiate replication, DNA synthesis was restored to 30% of control. This result suggested the presence of an activity in the extracts that reactivates *trans*-DDP-modified DNA templates for replication. This hypothesis was confirmed by an in vitro nucleotide excision repair assay that revealed activity in 293 and HeLa cell extracts selective for *trans*-DDP-modified plasmid DNAs. Such selective repair of *trans*-DDP-damaged DNA in human cells would contribute to its lack of antitumor activity.

An accepted mode of action for many anticancer drugs is the inhibition of DNA synthesis by drug–DNA adducts that impair the ability of polymerases to traverse the lesion. In mammalian cells, it has been very difficult to uncover the precise mechanism by which adducts functionally inactivate template DNA owing, in part, to the complexity of the replication apparatus. In the case of cisplatin, the major DNA adducts are intrastrand cross-links between N7 atoms of adjacent guanines or, at a lower frequency, adenine and guanine bases [for a review, see Sherman and Lippard (1987)]. These cross-links inhibit DNA polymerases and have been postulated to lead to the cytotoxic effects of the drug (Harder & Rosenberg, 1970; Howle & Gale, 1970).

Replication mapping experiments using both purified prokaryotic (Pinto & Lippard, 1985) and eukaryotic (Villani et al., 1988) DNA polymerases on single-stranded DNA templates have demonstrated the ability of *cis*-DDP[1] adducts to block the polymerases, although not without some translesion synthesis (Burstyn, Comess, and Lippard, unpublished results). We have been able to assess the effect of sequence context on the relative *cis*-DDP blockage sites by using bacteriophage T7 polymerase on double-stranded DNA (Burstyn, Heiger-Bernays, Essigmann, and Lippard unpublished results). Mapping experiments such as these and others examining different lesions (Moore et al., 1980; Rouet & Essigmann, 1985; Hayes & LeClerc, 1986; Gralla et al., 1987; Taylor & O'Day, 1990) can provide information regarding the influence of adducts on the activity of DNA polymerases.

In order to address the role of DNA-damaging agents on mammalian DNA replication, specifically the effects of a variety of platinum drugs in a biologically relevant milieu, we have employed an SV40-based in vitro replication system (Li & Kelly, 1984; Stillmann & Gluzman, 1985). This system utilizes soluble extracts from the cytoplasm of human cell lines that are capable of supporting efficient replication and supercoiling of exogenous plasmid templates containing the minimal SV40 origin of replication. All of the replication machinery is provided by the cytosolic extract with the exception of the viral protein, large T-antigen. In this initial study we have investigated three platinum compounds having different chemical properties and clinical efficacies. Specifically, we describe results for cisplatin and its clinically inactive isomer *trans*-DDP, both of which form intrastrand cross-links as their principal DNA lesions. We also examine the monofunctionally binding, antitumor-inactive compound [Pt-

† This work was supported by U.S. Public Health Service Grants CA34992 (to S.J.L.) and CA52127 and T32ES00597 (to J.M.E.).
‡ Department of Chemistry.
§ Whitaker College of Health Sciences and Technology.

[1] Abbreviations: DDP, diamminedichloroplatinum(II); dien, diethylenetriamine; SV40, simian virus 40; kbp, kilobase pairs; $(D/N)_b$, bound drug to nucleotide ratio; AAS, atomic absorption spectroscopy; form II, closed circular duplex DNA containing at least one single-stranded break; RI, replicative intermediates.

0006-2960/90/0429-8461$02.50/0